Atmosphere and Marginal-Sea Interaction Leading to an Interannual Variation in Cold-Air Outbreak Activity over the Japan Sea

ATSUHIKO ISOBE

Department of Earth System Science and Technology, Interdisciplinary Graduate School of Engineering Sciences, Kyushu University, Fukuoka, Japan

ROBERT C. BEARDSLEY

Physical Oceanography Department, Woods Hole Oceanographic Institution, Woods Hole, Massachusetts

(Manuscript received 17 November 2006, in final form 23 April 2007)

ABSTRACT

The interannual variation in cold-air outbreak activity over the Japan Sea is investigated using Japan Meteorological Agency buoy 21002 and Quick Scatterometer (QuikSCAT) wind data, Japan Oceanographic Data Center sea surface temperature (SST) data, NCEP–NCAR reanalysis surface wind and sea level pressure (SLP) data, and the winter Arctic Oscillation (AO) index of Thompson and Wallace. Cold-air outbreaks occur during the "winter" November–March period, and wind data for this season for the 19-winter period 1981–2000 were analyzed. Wavelet spectra averaged between 5- and 15-day periods were used to evaluate the intensity of cold-air outbreaks quantitatively. The winter mean wavelet spectra exhibited a clear interannual variation and a significant positive correlation with the AO index, indicating that intensive cold-air outbreaks frequently occur during relatively warm winters caused by a quasi-decadal AO. Based on the SST and SLP data, the low atmospheric surface pressure disturbances tend to develop over the warm East China Sea in warm winters in the positive AO phase. As these low SLP disturbances advance toward the northern Japan islands during the positive AO phase, they intensify more, leading to stronger cold-air outbreaks over the Japan Sea and increased sea surface cooling over the northern Japan Sea.

1. Introduction

In winter over the Japan Sea, one can often find a windy area extending southeastward from the narrow valley at Vladivostok, Russia. The January 2002 average surface wind speed (Fig. 1) is based on satellite scatterometer data downloaded from the Quick Scatterometer (QuikSCAT) Web site (http://podaac.jpl.nasa.gov/), and the wind rose (Fig. 1) is computed using wind data obtained at the Japan Meteorological Agency (JMA) weather buoy 21002 (located at the wind rose center; 37°45′N, 134°23′E). Wind direction probabilities are calculated every 10° using wind data faster than 5 m s^{-1} between 1 November and 31 March for the years 1981 to 2000. A strong wind band reaches the Noto Peninsula, Japan, even in the monthly-averaged field, and winds from the northwest are dominant. This strong southeastward wind band is formed by cold-air outbreaks that occur with an interval of about 6 days (Kawamura and Wu 1998). In addition to these "usual" outbreaks, the "very cold Siberian air outbreaks" (Dorman et al. 2004) occur 13.5 times on average during November through March (i.e., with a ~12-day interval).

Oceanographers as well as meteorologists have called attention to cold-air outbreaks over the Japan Sea. For instance, cold-air outbreaks can cause sufficient deepening of the surface mixed layer that may delay the onset of the spring phytoplankton bloom in the Japan Sea (Yamada et al. 2004; Onitsuka and Yanagi 2005). It is therefore reasonable to consider that interannual variations in the frequency and intensity of cold-air outbreaks may contribute significantly to biological variability in the Japan Sea. For the first time, this interannual variation in cold-air outbreak activity is investigated here using archived ocean and atmosphere

Corresponding author address: Atsuhiko Isobe, Department of Earth System Science and Technology, Interdisciplinary Graduate School of Engineering Sciences, Kyushu University, 6-1, Kasuga-Koen, Kasuga 816-8580, Japan.
E-mail: isobe@esst.kyushu-u.ac.jp

DOI: 10.1175/2007JCLI1779.1

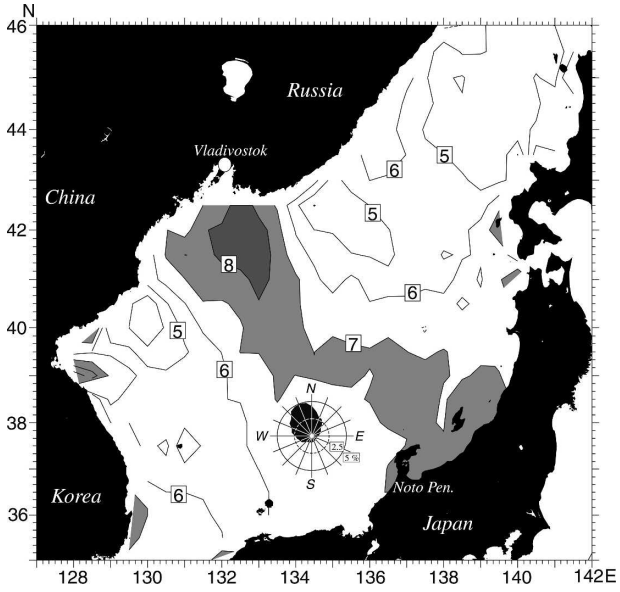

FIG. 1. Horizontal distribution of surface wind speed ($m\,s^{-1}$) averaged over January 2002. The data are derived from QuikSCAT observations. Contour interval is 1 $m\,s^{-1}$. The area with speed higher than 7 $m\,s^{-1}$ is stippled to emphasize cold-air outbreaks extending from Vladivostok. The inset panel shows the 19-yr winter wind rose obtained at JMA buoy 21002 located at the wind rose center.

datasets. A notable conclusion shown in section 5 is that cold-air outbreaks *strengthen* locally over the Japan Sea when the East Asian winter monsoon *weakens* in warm winters caused by the decadal Arctic Oscillation (AO; Thompson and Wallace 1998).

2. Data

Four datasets are used in analyzing the interannual variation of cold-air outbreaks. Each data source and processing method adopted for this study is presented next.

First, the wind data (wind speed and direction) collected on JMA weather buoy 21002 (Fig. 1) are used. These data are provided on a CD-ROM by the Japan Meteorological Business Support Center. In general, cold-air outbreaks occur from November through March (see Table 3a of Dorman et al. 2004), and so these five months are regarded as "winter" in this study. Although the buoy measurements started in 1978, wind data were often missing before 1981, likely due to mechanical problem. Thus, wind data from the 5-month November–March season are analyzed here over the 19-winter period from 1981 to 2000. The buoy wind data observed every 3 h were first averaged over each day. Since the observed winds are unidirectional, mostly directed toward the southeast as shown by the wind rose (Fig. 1), our analyses are focused on wind speeds regardless of wind direction.

Second, sea surface temperature (SST) is investigated in order to find the ocean response to the interannual variation in cold-air outbreaks. The SST data from the East China Sea as well as the Japan Sea for the November–March period from 1900 to 2000 (about 516 000 stations) were downloaded from the Japan Oceanographic Data Center (JODC) Web site (http://www.jodc.go.jp/). As shown later in section 4, SST over the East China Sea plays a key role in determining interannual variability of cold-air outbreaks in the Japan Sea. To investigate horizontal patterns, these SST data are converted into 0.5° latitude by 0.5° longitude gridded data using a Gaussian filter with an *e*-folding scale of 0.25° and a tail length of 0.5°. Before averaging the SST data in each grid cell, data that exceed 3 times the standard deviation from their average value are removed. In addition, any grid cell that has less than 10 data values is omitted. A combination of median and Laplacian filters is used to remove noisy patterns after gridding.

In addition to the above two datasets, the meteorological reanalysis dataset (Kalnay et al. 1996) provided by the National Centers for Environmental Prediction (NCEP)–National Center for Atmospheric Research (NCAR) from 1971 to 2000 is used to investigate the sea level pressure (SLP) fields over the study area. This NCEP–NCAR reanalysis dataset provides geopotential heights at 500 (Z_{500}) and 1000 (Z_{1000}) hPa at every 2.5° by 2.5° grid cell over the globe. These data are converted into SLP in hectopascals using the equation $1000 \times \exp(Z_{1000}/[1.542\,288\,5(Z_{500} - Z_{1000})]$. This SLP dataset from November through March is used in each winter.

Last, the AO index provided by Thompson and Wallace (1998) on their Web site (http://jisao.atmos.washington.edu/ao/) is used.

3. Interannual variation of cold-air outbreaks

a. Winds at JMA buoy 21002

Time series of wind speed at the JMA buoy during the 1985/86 and 1992/93 winters (Fig. 2) show that, while the average wind speeds (shown by the bold bar) in these two winters are similar, strong winds faster than 15 $m\,s^{-1}$ are observed only during the 1992/93 winter. It seems likely then that more intense surface mixed-layer modification occurred in the course of these intensive cold-air outbreak events during the 1992/93 winter. Thus, the frequency of intense outbreaks each winter should be a better index of annual

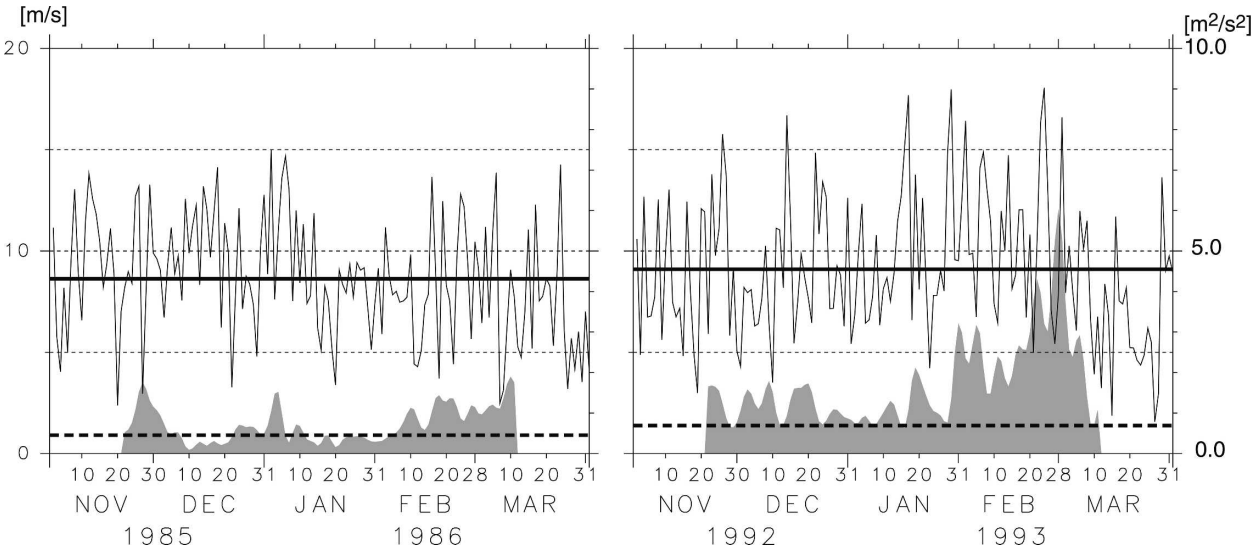

FIG. 2. Time series of the daily-averaged wind speed (m s^{-1}) at JMA buoy 21002 between November through March in (left) 1985/86 and (right) 1992/93. The two bold bars represent the mean values in each winter. The stippled areas represent the scale-averaged wavelet spectra (m^2 s^{-2}) between 5- and 15-day periods. See the right ordinate for their value. Wavelet spectra cannot be computed on either end because of the cone of influence (see Torrence and Compo 1998), and so the spectra in the first and last 20 days of the time series are omitted. The two broken bars represent the 95% confidence level.

outbreak activity than the average winter wind speed. Therefore, the "intensity" of winter outbreak events is quantified using wavelet analysis of the wind speeds at the JMA buoy.

The wavelet analysis shows remarkable outbreak signals between 5- and 15-day periods (not shown) as suggested by Kawamura and Wu (1998) and Dorman et al. (2004). Thus, the scale-averaged wavelet spectra (Fig. 2; Torrence and Compo 1998) are computed between these periods to cover the outbreak frequency band; the height of the stippled area represents the wavelet spectra. The initial 20 and last 20 days are left blank because these days are included in the cone of influence for the wavelet spectra at the 15-day period. However, intense cold-air outbreaks occur mainly between December and February (Dorman et al. 2004), and so the strongest winter outbreak events are included in the spectral time series. In total, the wavelet spectra in 1992/93 are much higher than those in 1985/86 even though wind speeds averaged over each winter are nearly the same. Thus, scale-averaged wavelet spectra are averaged over each winter (ignoring the 20-day gaps at each end), and these averaged spectra are used as representative values for each winter to investigate the interannual variation of cold-air outbreaks; the averaged spectra can be regarded as the variance in the selected frequency band (Torrence and Compo 1998).

The winter mean wind speeds from 1981 to 2000 are normalized by the maximum value during the 19-winter period (Fig. 3, upper panel). The range of interannual variation in averaged wind speeds is less than 20% of the maximum value, suggesting that winter mean wind speed is a poor index of interannual variability. However, a clear interannual variation in the winter mean wavelet spectra is detected. From the mean wavelet spectra normalized by the maximum value during the 19-winter period (Fig. 3, lower panel), two peaks are prominent, in early the 1980s and early 1990s, indicative of more intense cold-air outbreak activity during these times.

It is well known that the interannual variation in the strength of the East Asian winter monsoon is well correlated with AO indices (e.g., Gong et al. 2001). The atmospheric pressure difference is small between the Siberian high and Aleutian low in the positive AO phase (i.e., winters with the positive AO index). The East Asian winter monsoon therefore weakens in this AO phase, and vice versa. In fact, Gong et al. (2001) found that the positive (negative) AO phase results in a weak (strong) Siberian high, and hence high (low) surface air temperature over eastern China. Does this AO variability influence cold-air outbreak activity over the Japan Sea? The mean wavelet spectra and AO index time series (Fig. 3, lower panel) have a positive correlation (correlation coefficient $R = 0.46$, a significant value suggested by the t test with 95% confidence level), while the mean wind speed and AO are uncorrelated ($R = -0.04$). This result suggests the following question: Why is cold-air outbreak activity intensified frequently in "warm" winters over East Asia?

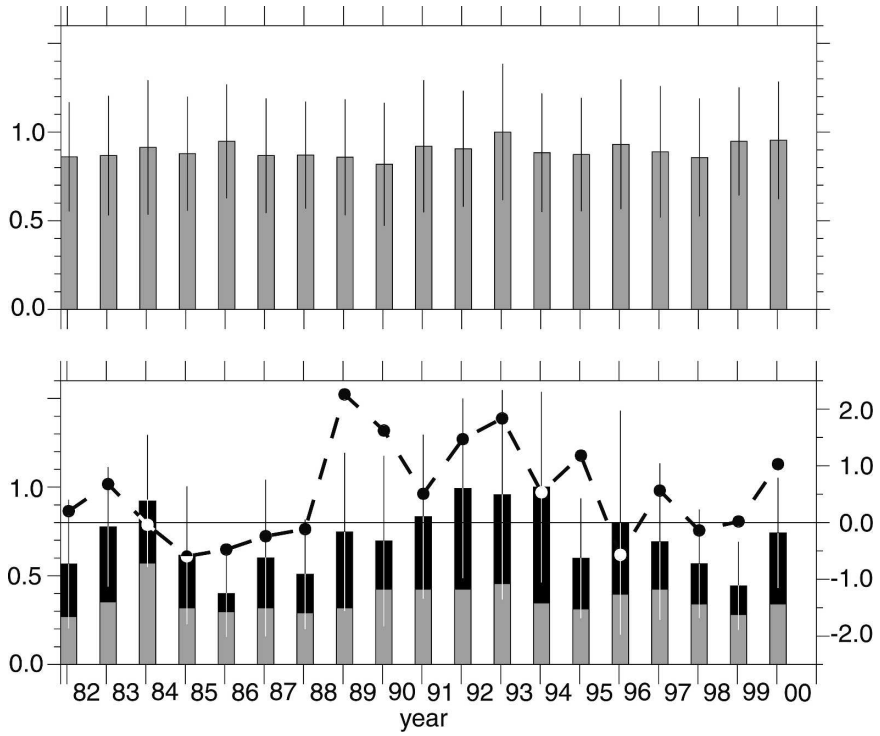

FIG. 3. Time series of the (top) wind speed and (bottom) scale-averaged wavelet spectra averaged over time between November through March in each year. The bars are normalized by the maximum values in the top and bottom panels, respectively. The standard deviations (thin lines) are also normalized by these maximum values. Portions exceeding the 95% confidence level are filled in with black on each bar of the bottom panel. The solid circles in the bottom panel represent the AO index averaged from November through March in each year. See the right ordinate for AO index scale. The broken line highlights the interannual variation of AO.

b. SST over the East Asian marginal seas

A relationship between AO and SST over East Asian marginal seas is next investigated before answering the above question. The SST data before gridding are divided into two groups, those taken in the positive AO phase (Fig. 4, upper panel), and those in the negative AO phase (Fig. 4, lower panel). Both panels show the anomaly fields from the winter SST averaged over the 101-yr dataset.

Following the conclusion of Gong et al. (2001), SST is relatively high (low) over the East China Sea in the positive (negative) AO phase. The SST anomaly in the Kuroshio region along the shelf break (denoted by the 200-m isobath in the East China Sea) is smaller than that on the shelf regardless of the AO phase. Thus, it is concluded that the temperature variation over the East China Sea is not due to the onshore heat transport from the Kuroshio region, but due to variation in the surface heat flux. These temperature variations over the East China Sea extend toward the southwestern Japan Sea because the ocean currents over the shelf are directed northeastward, and because the currents flow into the Japan Sea as the Tsushima Warm Current (Isobe 1999; Katoh et al. 2000). In addition, the surface heat flux may change with AO over the southwestern Japan Sea as well as the East China Sea. Hence, a positive (negative) SST anomaly is detected in the southwestern Japan Sea during the positive (negative) AO phase.

However, note that the above anomalous distribution of SST is limited to the southwest of the Noto Peninsula on which cold-air outbreaks strike. In addition, the temperature anomalies in both positive and negative AO phases are reversed in the Tsushima Warm Current downstream northeast of the Noto Peninsula. This relationship is consistent with the observed fact that the cold-air outbreak is enhanced in warm winters (i.e., the positive AO phase) because the enhanced outbreak must cause the intense sea surface cooling. Note that the sea surface heat flux is directed to the atmosphere over East Asian marginal seas during winter (Hirose et al. 1996, 1999).

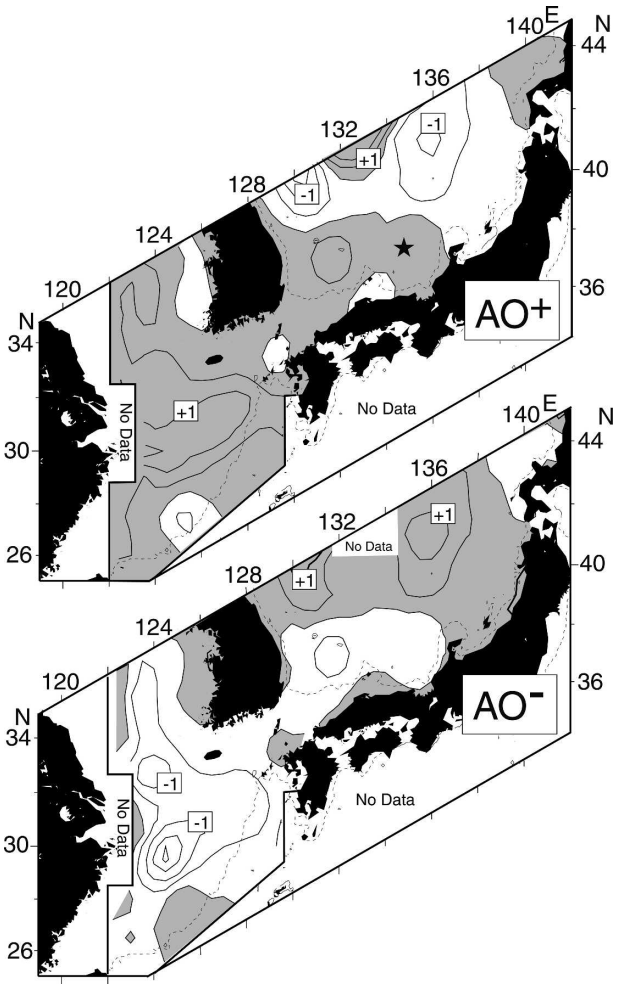

FIG. 4. Horizontal distributions of gridded SST in the (top) positive (marked as AO+) and (bottom) negative (AO−) AO phases. Both panels denote anomaly fields from the climatological values in the past 101 yr. The contour interval is 0.5°C. The areas with the positive anomaly are stippled. The star in the top panel denotes the location of JMA buoy 21002. Note that SST anomalies are not depicted south of the Japan islands and south of the bold line in the East China Sea. Grid cells that have less than 10 data values are also omitted (shown by "no data"). The 200-m isobath is shown by thin broken lines.

Minobe et al. (2004) also investigated the SST decadal variation over the Japan Sea, and found a phase difference of 60° to 90° between the southwestern and northeastern Japan Sea for the decadal complex EOF first mode. Indeed, it is difficult for the present analysis using the composite SST maps (Fig. 4) to compute the phase difference accurately in the Japan Sea. However, their result may be consistent with the present study showing that the decadal SST variations have different phases between the southwestern East China Sea and northeastern Japan Sea.

4. Air–sea interaction over the East Asian marginal seas

Why are cold-air outbreaks more frequent and intense in warm winters? To answer this question, winter SLP patterns are investigated using the NCEP–NCAR reanalysis dataset. SLP must be low over the northern Japan islands whenever a cold-air outbreak occurs. The origin of these synoptic-scale atmospheric disturbances causing outbreaks is next investigated.

The spatial distribution of cross-correlation coefficients between SLP at a reference point and surrounding areas including the North Pacific is examined (Fig. 5). To extract the atmospheric disturbances associated with cold-air outbreaks, SLPs are bandpassed between 5 and 15 days using a Butterworth filter before computing the cross-correlation coefficients. Two reference points (see stars in the upper panels) are chosen on the western and eastern sides of the northern Japan islands. The panels denote the cross-correlation coefficients over the study area at the same time, and the coefficients for the previous 1, 2, and 3 days, respectively.

The cross-correlation coefficients at the same time (top panels of Fig. 5) show that the SLP disturbances over the northern Japan islands have a synoptic scale of ~1000–1500 km. The wind directions at the JMA buoy 21002 are mostly southeastward (Fig. 1), so it is likely that the SLP disturbances represent low pressures mostly. Highly correlated areas over the Japan Sea are found for 1 day before, and areas close to the Korean Peninsula are found for 2 days before, regardless of where the reference point is set. The panels for 3 days before show that atmospheric disturbances over the northern Japan islands originate mainly from the East China Sea, where the SST changes considerably depending on the AO phase.

Standard deviations of the bandpassed SLP between the positive (σ_+) and negative (σ_-) AO phases are next compared (Fig. 6) using the horizontal distribution of the ratio, $(\sigma_+ - \sigma_-)/\sigma_- \times 100$. Only positive contours are depicted because the positive values mean that SLP varies intensely in warm winters with the positive AO index. For reference, the areas with cross-correlation coefficients higher than 0.4 for the 1, 2, and 3 days before, respectively, are examined for the point centered in Japan Sea. The significant (F test with 99% confidence level) positive area extends into the East China Sea and southern Japan Sea. This result means that SLP disturbances advancing northeastward are amplified over these ocean regions in the positive AO phase. Thereby, as suggested by Figs. 5 and 6, the following scenario prevails: the high SST in the positive

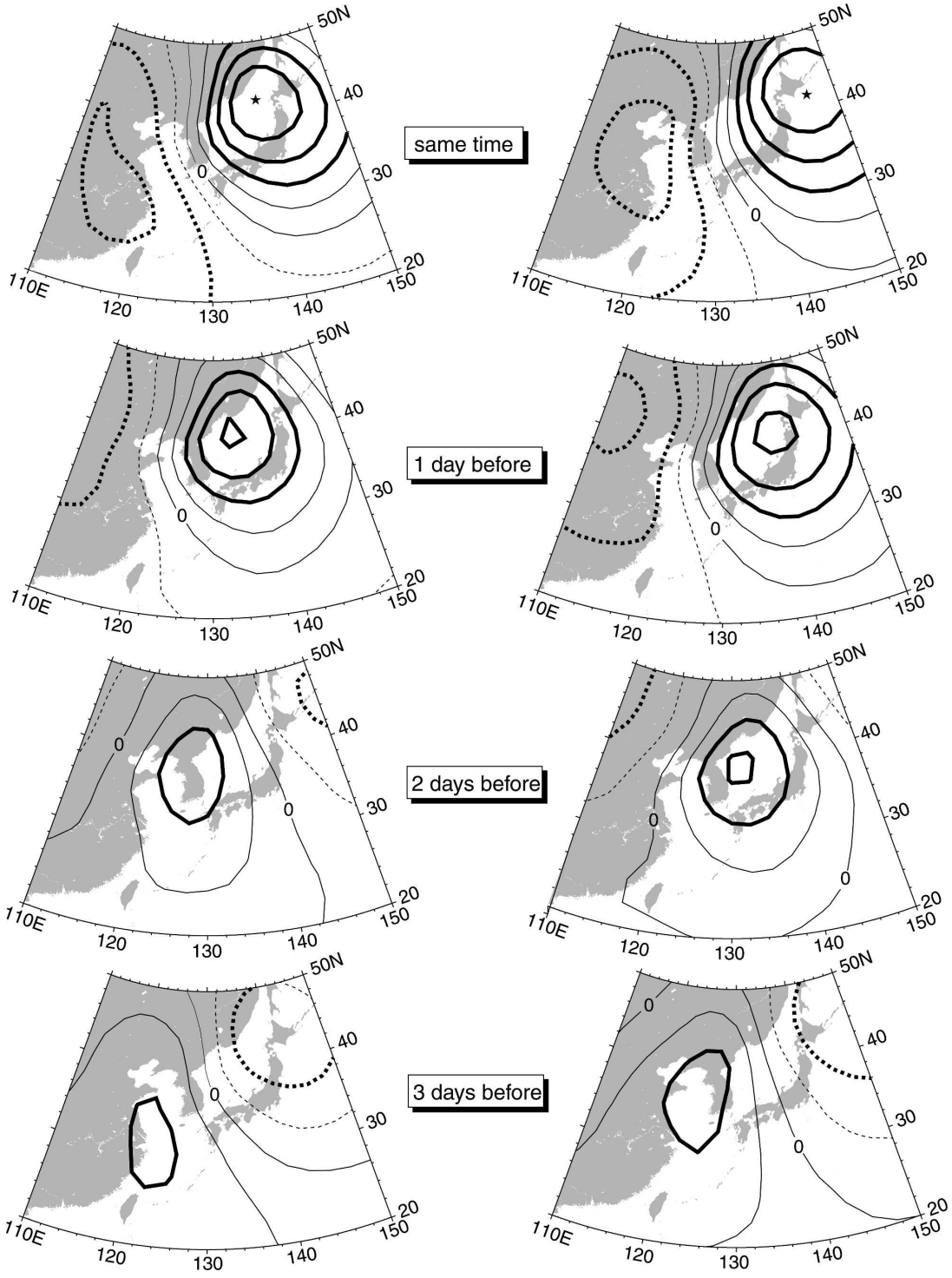

FIG. 5. Horizontal maps of the cross-correlation coefficients computed between SLPs at the reference point and surrounding areas. Two reference points are chosen as shown by the stars in the top two panels. The sequential maps for 1, 2, and 3 days before the time of the top panels are shown in the left and right panels, respectively, for each reference point. Dotted lines are used for negative values. Bold lines are used for the absolute value of the coefficients higher than 0.4, which is a significant value suggested by a *t* test with 99% confidence limit.

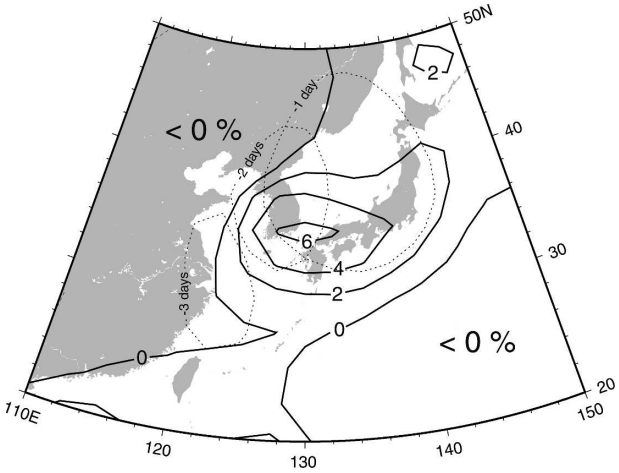

FIG. 6. Horizontal distribution of the ratio $(\sigma_+ - \sigma_-)/\sigma_- \times 100$, where σ_+ and σ_- denote the SLP standard deviations in the positive and negative AO phases, respectively. Also shown are the areas with cross correlations higher than 0.4 for the reference point on the western side of the northern Japan islands. Contour lines 1, 2, and 3 days before are depicted by dotted lines.

AO phase triggers the generation of low SLPs over the East China Sea, and that low SLPs advancing toward the northern Japan islands intensify cold-air outbreaks over the Japan Sea. In fact, Xie et al. (2002) suggest that the SST increase over the Yellow and East China Sea shelves causes the low SLP, and that the resultant SLP field leads to the wind field adjustment as found in satellite observations. However, the relationship between the storm development and SST gradient across the Kuroshio front (Xie et al. 2002) is unclear in the present analysis, presumably due to the relatively coarse grid in Fig. 4. Nevertheless, the low SLPs are likely to strengthen when advancing over the East Asian marginal seas because the atmosphere gains heat over these areas during winter (Hirose et al. 1996, 1999). The cold-air outbreaks result in sea surface cooling, and so it is reasonable that SST northeast of the Noto Peninsula is relatively low in spite of the warm winter in the positive AO phase.

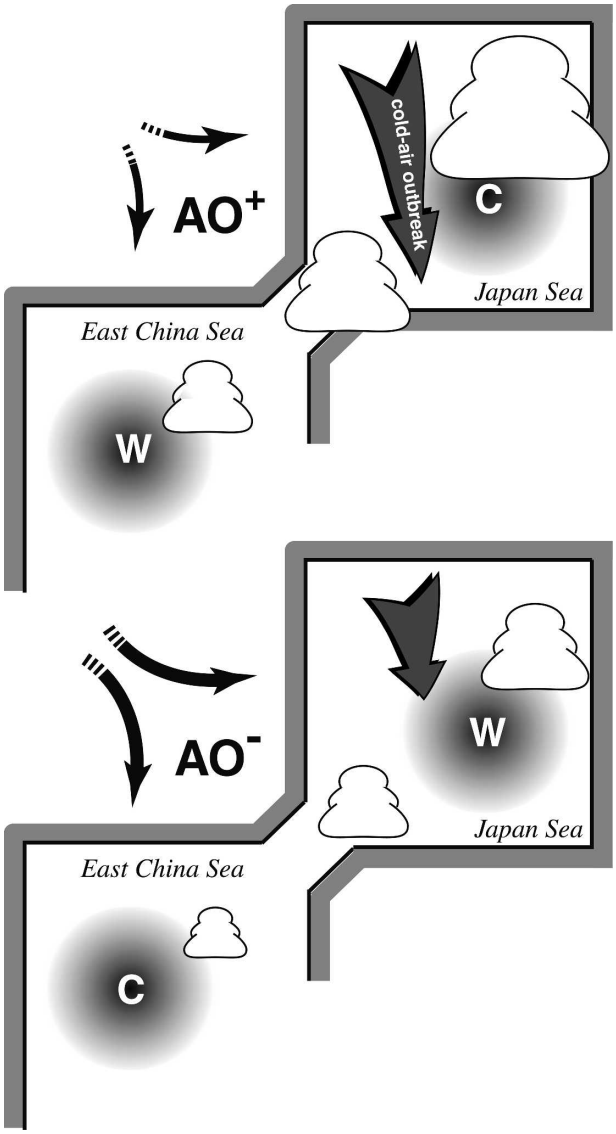

FIG. 7. Schematic view of the atmosphere and marginal-sea interaction leading to the interannual oscillation of the cold-air outbreaks over the Japan Sea. The letters W and C denote the warm and cool SST, respectively. The growth of low SLP distributions as they move toward the northeast is expressed by the size of the cloud cartoons.

5. Conclusions

Our conclusions are summarized schematically (Fig. 7). SST over the East China Sea is high in warm winters in the positive AO phase. The low SLP develops on the warm East China Sea and advances toward the northern Japan islands. The enhanced atmospheric disturbances in the positive AO phase lead to more intense cold-air outbreaks, which cause the low SST in the northern Japan Sea. In contrast, severe winters reduce SST over the East China Sea in the negative AO phase, and so the cold-air outbreaks are suppressed because the cool East China Sea diminishes the atmospheric disturbances advancing toward the northern Japan islands. Thus, the decadal and global AO variability affects the intensity in the regional cold-air outbreaks over the Japan Sea through the interaction between the atmosphere and marginal seas. The warm (cool) East China Sea therefore makes the northern Japan Sea cool (warm) through this atmosphere and marginal-sea interaction.

Acknowledgments. The authors express their sincere thanks to Tomoharu Senjyu for his valuable suggestions and encouragement and to Clive Dorman for his introduction to this topic. Comments of two anonymous reviewers and the editor were helpful in improving the manuscript.

REFERENCES

Dorman, C. E., R. C. Beardsley, N. A. Dashko, C. A. Friehe, D. Kheilf, K. Cho, R. Limeburner, and S. M. Varlamov, 2004: Winter marine atmosphere conditions over the Japan Sea. *J. Geophys. Res.,* **109,** C12011, doi:10.1029/2001JC001197.

Gong, D.-Y., S.-W. Wang, and J.-H. Zhu, 2001: East Asian winter monsoon and Arctic Oscillation. *Geophys. Res. Lett.,* **28,** 2073–2076.

Hirose, N., C.-H. Kim, and J.-H. Yoon, 1996: Heat budget in the Japan Sea. *J. Oceanogr.,* **52,** 553–574.

——, H.-C. Lee, and J.-H. Yoon, 1999: Surface heat flux in the East China Sea and the Yellow Sea. *J. Phys. Oceanogr.,* **29,** 401–417.

Isobe, A., 1999: On the origin of the Tsushima Warm Current and its seasonality. *Cont. Shelf Res.,* **19,** 117–133.

Kalnay, E., and Coauthors, 1996: The NCEP/NCAR 40-Year Reanalysis Project. *Bull. Amer. Meteor. Soc.,* **77,** 437–471.

Katoh, O., K. Morinaga, and N. Nakagawa, 2000: Current distributions in the southern East China Sea in summer. *J. Geophys. Res.,* **105,** 8565–8573.

Kawamura, H., and P. Wu, 1998: Formation mechanism of Japan Sea Proper Water in the flux center off Vladivostok. *J. Geophys. Res.,* **103,** 21 611–21 622.

Minobe, S., A. Sako, and M. Nakamura, 2004: Interannual to interdecadal variability in the Japan Sea based on a new gridded upper water temperature dataset. *J. Phys. Oceanogr.,* **34,** 2382–2397.

Onitsuka, G., and T. Yanagi, 2005: Differences in ecosystem dynamics between the northern and southern parts of the Japan Sea: Analyses with two ecosystem models. *J. Oceanogr.,* **61,** 415–433.

Thompson, D. W. J., and J. M. Wallace, 1998: The Arctic Oscillation signature in the wintertime geopotential height and temperature fields. *Geophys. Res. Lett.,* **25,** 1297–1300.

Torrence, C., and G. P. Compo, 1998: A practical guide to wavelet analysis. *Bull. Amer. Meteor. Soc.,* **79,** 61–78.

Xie, S.-P., J. Hafner, Y. Tanimoto, W. T. Liu, H. Tokinaga, and H. Xu, 2002: Bathymetric effect on the winter sea surface temperature and climate of the Yellow and East China Seas. *Geophys. Res. Lett.,* **29,** 2228, doi:10.1029/2002GL015884.

Yamada, K., J. Ishizaka, S. Yoo, H.-C. Kim, and S. Chiba, 2004: Seasonal and interannual variability of sea surface chlorophyll *a* concentration in the Japan/East Sea (JES). *Prog. Oceanogr.,* **61,** 193–211.